City Research Online

City St George's, University of London

Citation: Uthman, M., Rahman, B. M., Kejalakshmy, N., Agrawal, A., Abana, H. & Grattan, K. T. V. (2012). Stabilized large mode area in tapered photonic crystal fiber for stable coupling. IEEE Photonics Journal, 4(2), pp. 340-349. doi: 10.1109/jphot.2012.2188788

This is the unspecified version of the paper.

This version of the publication may differ from the final published version. To cite this item please consult the publisher's version.

Permanent repository link: https://openaccess.city.ac.uk/id/eprint/1243/

Link to published version: https://doi.org/10.1109/jphot.2012.2188788

Copyright and Reuse: Copyright and Moral Rights remain with the author(s) and/or copyright holders. Copies of full items can be used for personal research or study, educational, or not-for-profit purposes without prior permission or charge, unless otherwise indicated, provided that the authors, title and full bibliographic details are credited, a hyperlink and/or URL is given for the original metadata page and the content is not changed in any way. For full details of reuse please refer to City Research Online policy.

City Research Online: http://openaccess.city.ac.uk/ publications@citystgeorges.ac.uk

Stabilized Large Mode Area in Tapered Photonic Crystal Fiber for Stable Coupling

M Uthman, B M A Rahman, N Kejalakshmy, A Agrawal, H Abana and K T V Grattan

City University London, School of Engineering and Mathematical Sciences, Northampton Square, London EC1V 0HB, UK

b.m.a.rahman@city.ac.uk

©2012 IEEE

Abstract: A rigorous modal solution approach based on the numerically efficient finite element method has been used to design a tapered Photonic Crystal Fibre with a large mode area that could be efficiently coupled to an optical fiber. We report here for the first time that the expanded mode area can be stabilized against possible fabrication tolerances by introducing a secondary surrounding waveguide with larger air-holes in the outer ring. A full-vectorial **H**-field approach is employed to obtain mode field areas along the tapered section and the Least Squares Boundary Residual (LSBR) method is used to obtain the coupling coefficients to a butt-coupled fiber.

Index Terms photonic crystal fiber, coupling, mode area, single mode fiber.

1. Introduction

A wide range of photonic crystal fibers (PCF) [1,2] can be used as potential waveguides and devices which may exploit their characteristics of being single moded, having higher modal birefringence and offering adjustable spot-size and dispersion properties which may be tailored for various linear and nonlinear applications. Initially PCF was considered to be an endlessly single mode fiber, but later numerical studies such as using the multipole method and the finite element method, have revealed that the cutoff conditions are critically controlled by the diameter to pitch ratio [3,4,5]. Their Mode Field Areas (MFA) are controllable and thus able to achieve both large and small spot-sizes. As an example, PCFs with smaller MFAs can be envisaged by enhancing their power density and tailoring their dispersion properties for various nonlinear applications, such as supercontinuum generation. Such a PCF with small core can also allow easy access to the evanescent fields for the design of optical sensors.

However, practical difficulties related to achieving efficient coupling of a PCF with a smaller MFA to the input/output sections have often been considered as creating a serious drawback in PCF technology. Unlike fusion splicing in conventional Single Mode Fiber (SMF), joining a PCF is difficult as the integrity of the air-holes is difficult to preserve, even though several recent efforts in for fusion splicing of a PCF to a SMF have been reported [6,7,8]. However, to obtain a low-loss coupling is particularly challenging due to the large mismatch between the MFA of a PCF and that of a SMF. A short gradient index fiber lens has also been considered [9] by incorporating this component between the two coupling sections with different MFAs. Use of a fused biconical taper, often used for a passive fiber coupler, has also been envisaged by placing a PCF and a pre-tapered SMF side by side and twisting and tapering them for efficient evanescent coupling [10]. A PCF can also be tapered adiabatically to adjust its MFA [1, 12]. As example, if the up-tapered part has a larger width near the end, its MFA increases and the coupling loss to a SMF can be relatively low, as reported in the literature [13,14]. However, these terminal sections with a large core dimension are likely to be multimoded which could also restrict the flexibility of the PCF designs. On the other hand, if the dimensions of a tapered PCF are adiabatically reduced, when the core mode approaches cutoff, the MFA would also increase. PCFs have been routinely tapered to control their dispersion properties with their pitch reduced from 3.0 μm to 500 nm [15], and even below 300 nm [16].

When a PCF is operating near the cutoff condition, as the pitch is reduced, this leads to the expansion of the mode field into the air cladding region [17]. This could expand the MFA to a size similar to that of a SMF which would make coupling between them easier. For this purpose, a PCF section can be tapered to bring it close to the cutoff condition. However, as it expands very rapidly in this region, it may be difficult to control as any small fabrication errors can make the MFA unstable when it expands exponentially. A similar problem exists in coupling a laser beam with a small asymmetric shape to a SMF with a larger circular beam profile. In that context, monolithically integrated spot-size converters (SSC) have been reported [18,19], designed to transform the spot-size of the output laser beam to allow for efficient coupling. To control the MFA with its fabrication tolerances, it is suggested here, for the first time, that a secondary guide can be considered. This approach is evaluated by using a rigorous full-vectorial finite element method (FEM) and the Least Squares Boundary Residual (LSBR) method. It is also shown here that the MFA can be stabilized, this being to account for the changes that may occur during the manufacturing processes of a tapered PCF. Coupling between waveguide sections with different spot-sizes have been a consistent problem, such as for photonic crystals [20], plasmonic waveguides [21,22] and efficient light extraction [23,24], where the approach presented here, the use of tapered guided wave section, can be considered.

1.1 THEORY

The coupling losses are caused by the mismatch of the MFAs and changes in the effective indices between the coupling sides. A typical approach to reduce the coupling loss would be to transform the MFA of one side adiabatically to achieve a better matching. If the changes are implemented slowly compared to the diffraction angle then the terminal MFA would give a clear indication of coupling efficiency enhancement. Hence, an accurate mode solver could be used to find the MFA of a tapered PCF rather than a beam evolutionary approach [10,13] or a time-domain approaches [12], which are computationally more expensive.

In the modal solution approach based on the FEM, the intricate cross section of the PCF can be accurately represented using many triangles of different shapes and sizes [25,26]. This flexibility makes the FEM preferable when compared to the finite difference method (FDM) which not only uses inefficient regular spaced meshing, but also cannot represent slanted or curved dielectric interfaces. The optical modes in a high contrast PCF, with two-dimensional confinement, are also hybrid in nature, with all six components of the **E** and **H** fields being present. It is also known that modal hybridness is enhanced by the presence of slanted or curved dielectric interfaces. Hence only a vectorial formulation can accurately represent their modal solutions and also the need for an accurate representation of the circular air-holes. In the present approach, a **H**-field based rigorous full-vectorial FEM has been used to analyze the operation regime of PCFs with air-holes arranged in a triangular lattice in the silica cladding. The **H**-field formulation [25] with the augmented penalty function technique is given below:

$$\omega^2 = \frac{\left(\int (\nabla\times\vec{\mathbf{H}})^*\cdot\hat{\varepsilon}^{-1}(\nabla\times\vec{\mathbf{H}})\,d\Omega\right)+\left(\int(\alpha/\varepsilon_0)(\nabla\cdot\vec{\mathbf{H}})^*\,(\nabla\cdot\vec{\mathbf{H}})\,d\Omega\right)}{\int\vec{\mathbf{H}}^*\cdot\hat{\mu}\,\vec{\mathbf{H}}\,d\Omega} \qquad (1)$$

where $\vec{\mathbf{H}}$ is the full-vectorial complex magnetic field, $\hat{\varepsilon}$ and $\hat{\mu}$ are the permittivity and permeability, respectively of the waveguide, ε_0 is the permittivity of the free space, ω^2 is the eigenvalue, where ω is the angular frequency of the wave and α is a dimensionless parameter used to impose the divergence-free condition of the magnetic field in a least squares sense. In this formulation both the $\hat{\varepsilon}$ and $\hat{\mu}$ parameters can be arbitrary complex tensors with possible off-diagonal coefficients, suitable to characterize electro-optic, acousto-optic and elasto-optic devices.

Finally, to analyze the coupling between a PCF and an optical fiber, the overlap integral method can be used to find the transmission coefficients and a simpler impedance-based approach can be used to find the reflection coefficients at the junction interfaces. However, it has been shown that the Least Squares Boundary Residual (LSBR) method [19,27] is rigorously convergent and it also can be used to obtain both the transmission and reflection coefficients by considering all the guided and discretized radiation modes of the structures. This LSBR method has been used here to find the power coupling between a butt coupled PCF and conventional optical fibers. On the hand, a versatile FDTD [33] approach can also be used to study scattering coefficients at a junction, but this approach is numerically very expensive.

2. Results

2.1 ANALYSIS OF A SMF

In this paper, the MFA is studied in some detail; however it is important to note that there have been various alternative definitions to represent this particular parameter. The MFA can be represented by the spot-size, σ, the effective area, A_{eff} and the Area second moment of intensity, A_{SMI}. The spot-size is usually defined as the area where the field intensity falls to $1/e$ of its maximum value (or where power intensity is $1/e^2$) [18,19]. The effective area, $A_{eff} = ((\int_i |E_i|^2)dA)^2 / (\int_i |E_i|^4 dA))$, where E is the electric field amplitude [29]. The Area second moment of the optical intensity $A_{SMI} = 2\sqrt{((\int x^2 I(x,y)/(\int I(x,y)))}$, where I(x,y) is the second moment of the intensity distribution profile [30]. Initially, a simple circular fiber is considered to study its MFA. The refractive indices of the silica cladding and the Ge-doped core are taken as 1.445 and 1.4502 respectively at the operating wavelength of 1.55 μm. Since, the TE and TM modes are degenerate; only the quasi-TM mode (with the dominant H^x and E^y fields) is considered in this analysis.

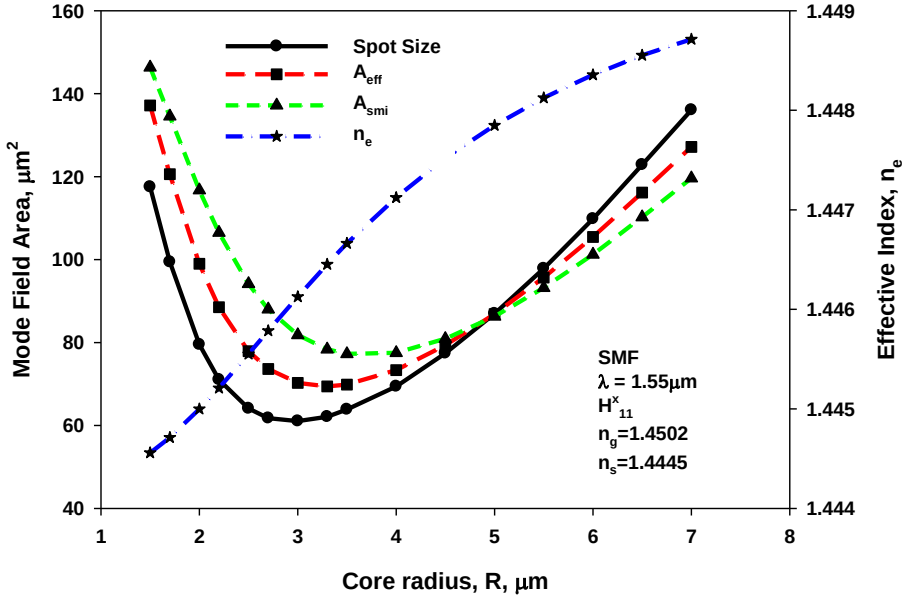

Fig. 1: Variation of mode field area and effective index of a SMF against core radius, R.

The variations of the effective index and the different MFAs with the core radius for this optical fiber are shown in Fig. 1. The effective index is defined as $n_e = \beta/k_o$, where β is the propagation constant and the wavenumber $k_o = 2\pi/\lambda$. It is shown that as the core radius is reduced, the effective index is monotonically reduced. Several MFA designs were studied carefully for different core radii. As the core radius is reduced, initially the MFAs reduce but as cutoff region approaches, the MFAs begin to increase again. However, their values and expansion regimes are slightly different. The values for these mode field areas were slightly different but they become identical at R = 5.0 μm. A SMF often has a radius of between 4.5 and 5.0 μm. A closer investigation has revealed that the field profile at R = 5.0 μm closely follows a Gaussian profile and this suggests that for a Gaussian shaped field profile, all the different MFA definitions may lead to a similar value. However, when the radius was larger than 5.0 μm, it was observed that in the field decay rate in the cladding was faster than its equivalent Gaussian profile suggests. Similarly, for a radius smaller than 5.0 μm, the field decays slowly in the cladding region compared to its equivalent Gaussian fitting profile. Thus an MFA defined by different approaches will likely have different values when the mode field is not Gaussian in shape.

2.2 ANALYSIS OF A TAPERED PCF

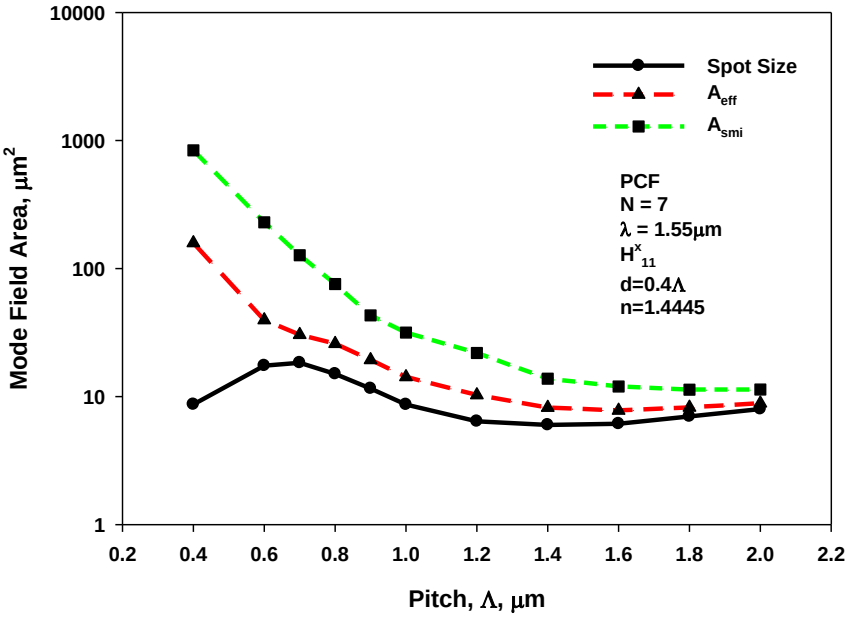

Fig. 2: Variation of mode field areas of a PCF against the pitch, Λ.

In this section, the MFA of a PCF, the main subject of this research, is thoroughly investigated. The PCF considered here has a number of rings, N (where in this case N = 7) and its silica refractive index is taken as 1.445 at the operating wavelength of 1.55 μm. The pitch, Λ, is varied from 2.0 to 0.4 μm with an air-hole diameter, d = 0.4Λ. Variations of the different MFA parameters with the pitch length, Λ, are shown in Fig. 2. The log scale is used for the MFA to cover the lower range more clearly. As the radius is reduced, the MFA initially reduces but then begins to increase again. It can be seen that all these parameters increase as the modal cutoff is approached; however, its spot-size, σ, also shows saturation. It should be noted that for a low-index contrast SMF, the modal field reduces monotonically in the cladding. However, due to the presence of air-holes in a PCF, the field profile does not decay monotonically outside the core region. In the definition of the spot-size, only the localized field values are considered, whereas the A_{eff} and A_{SMI} use the integration of field profile and these are more stable. Although, these values give some indication of their MFAs and are useful to identify the size for optimum coupling, to calculate the coupling efficiency the rigorous LSBR approach will be used.

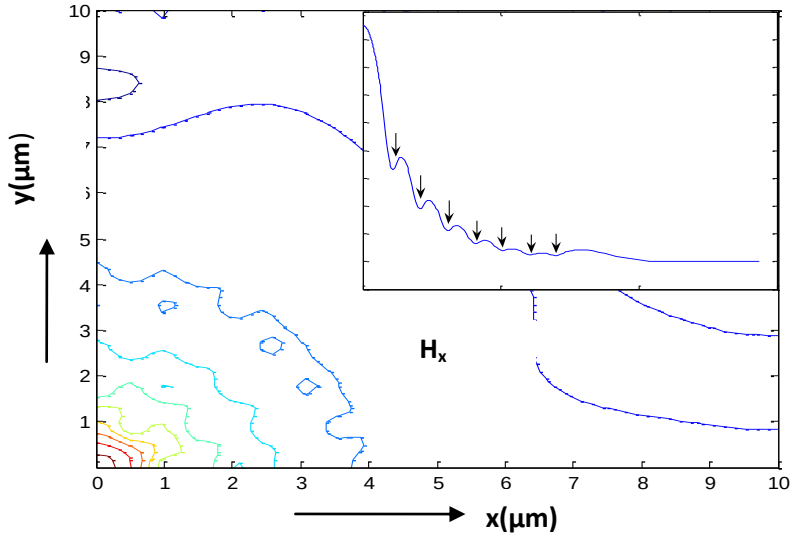

Fig. 3: H_x field profile of the H^x_{11} mode for N = 7, Λ = 1.0, d/Λ = 0.4, and d_7/Λ=0.8.

The H_x field profile for the H^x_{11} mode is shown in Fig. 3 for a PCF with 7 air-hole rings, when Λ = 1.0 μm and for all the rings d/Λ = 0.4 and except for the last ring where d_7/Λ = 0.8. It can be observed that the field contours are not concentric circles, but show 'cheese-like' holes due to the presence of the air-holes. The variation of the H_x along the x-axis is also shown as an inset, clearly demonstrating the field variations are not monotonic and the location field minima around the air-holes are shown by arrows. Hence, the simple spot-size, which depends on the local field values, can be unreliable when used to describe the MFA of a PCF. Subsequently to gauge the field expansion, the term A_{eff} is used in this work.

Variations of the effective areas, A_{eff}, with the pitch for a PCF with 5 air-hole rings are shown in Fig. 4. Here the effect of the field expansion for two different air-hole ratios, d/Λ, are shown, besides the effect of having a larger air-hole in the last ring (which also is shown). When all the air-holes are of identical diameter and either 0.4Λ or 0.5Λ, the value of A_{eff} increases exponentially as Λ is reduced. It can be observed that for a smaller d/Λ = 0.4, the effective area, A_{eff} becomes higher due to the smaller size of the air-holes compared to that where d/Λ = 0.5. It can also be observed that as larger air-holes were introduced in the outermost ring (5^{th} ring)(shown as an inset), the value of the MFA is forced to remain flatter than it would have been otherwise at lower values of pitch. In the case of d/Λ = 0.4, all the air-holes in the first 4 rings have their dimension, d = 0.4Λ, except the 5^{th} ring which has a larger dimension, denoted by d_5 = 0.8Λ. This ensures that the MFA is stable at the lower pitch values without it expanding exponentially and the mode expansion slows down by the last ring, which has larger air-holes. This would allow stable coupling to occur without much error or uncertainty even if there were structural variations occurring during the fabrication or tapering. This figure also demonstrates that a PCF with smaller air-holes in most of the inner rings and larger air-holes in the last ring is expected to produce a larger A_{eff}, which is also reasonably stable with the pitch variation. There are also some random variations which occur due to mode degeneration with the cladding modes [31].

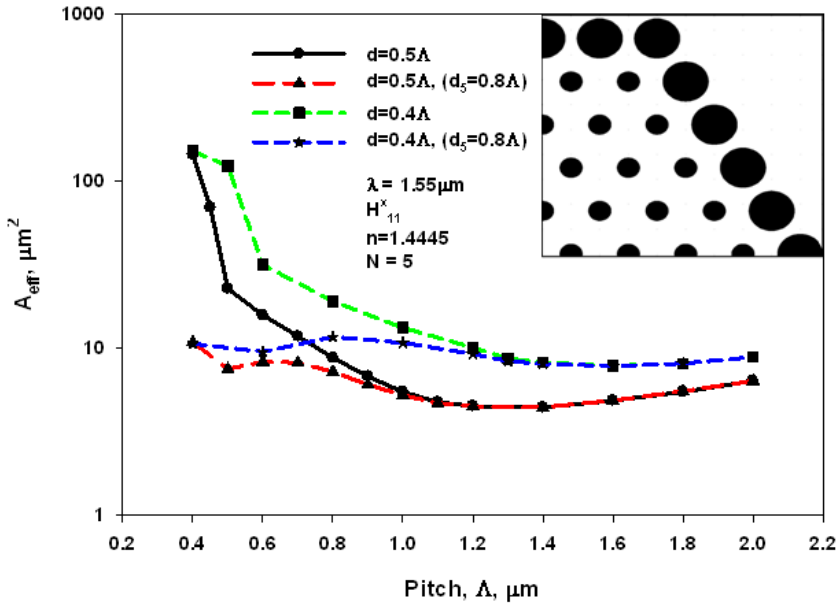

Fig. 4: Variations of the A_{eff} with the pitch length for PCF having d/Λ = 0.4 and 0.5 for N = 5

Next, the variations of the effective areas, A_{eff}, with the pitch are shown in Fig. 5 for two different numbers of air-hole rings, given by N = 5 and 7. In both cases, d/Λ is taken as 0.4 and additional curves are also shown when the air-hole diameter in the last ring is increased to 0.8Λ. It can be noted that when all the air-hole diameters are of the same size for all the rings, the value of A_{eff} increases progressively as the pitch, Λ, is reduced. When the number of rings is large, the value of A_{eff} is slightly larger as there is a larger cladding region available into which the mode can expand. It is also shown in Fig. 5 that by using 7 rings (N = 7) and having the same diameter air-holes in the last ring (7^{th}), a higher A_{eff} value can be obtained, but this would be very sensitive to the pitch value. However, as the air-hole diameter of the last ring is increased, in both cases, the value of A_{eff} stabilizes. It can be also noted here that this A_{eff} value is stable when the air-hole diameter in the last ring is large, where d = 0.8Λ and with a smaller value of the pitch, A_{eff} shows a lower variation with the pitch. This suggests that if the terminal dimension of a tapered PCF is taken as Λ = 0.7 μm, a smaller variation of pitch due to the fabrication tolerances would not change A_{eff} significantly. For N = 7, when all the air-holes in the first 6 rings have a dimension, d = 0.4Λ (except the air-holes in the 7^{th} ring with the dimension of d_7 = 0.8Λ), the stabilized value of MFA is around 20 μm^2.

As can be observed, when the number of rings in the cladding, N, is increased, this results in an increase in the MFA as well. This shows that with a higher number of rings it is possible to achieve a very high MFA that is comparable to that of SMF or if needed to be comparable to that of an erbium doped fiber amplifier (EDFA); this would then result in a lowering of the insertion loss when butt-coupled to these fibers.

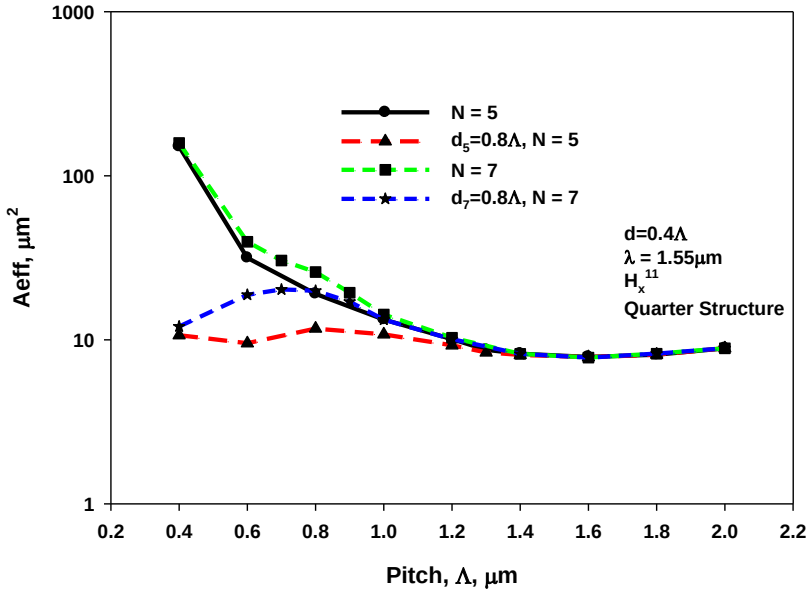

Fig. 5: Variations of the A_{eff} with the pitch length for PCF having $d/\Lambda = 0.4$ for N = 5 and N = 7.

2.3 COUPLING BETWEEN PCF AND OPTICAL FIBER

Finally, the Coupling Efficiency is calculated rigorously by using the Least Squares Boundary Residual (LSBR) method [27]. In Fig. 5, it was shown that a stable value of A_{eff} = 20 μm can be obtained for N = 7 with all the air-hole diameters, $d = 0.4\Lambda$ except that of the last ring, where $d_7 = 0.8\Lambda$. A typical Erbium Doped Fiber Amplifier (EDFA) may have an A_{eff} value around 25 μm^2 and a SMF have its A_{eff} around 80 μm^2. Thus a tapered PCF with N = 7, $d/\Lambda = 0.4$ and a final (7^{th}) hole ratio $d_7/\Lambda = 0.8$ μm, as shown above, could be efficiently coupled to an EDFA, or a lensed fiber with a similar MFA.

The variations of the Coupling Efficiency with the pitch length for a PCF with 7 rings are shown in Fig. 6 when it is butt-coupled to an EDFA. In this case the core and cladding indices of the EDFA are taken to be 1.46178 and 1.445, respectively and its radius is taken as 2.5 μm. When all the air-holes are equal to 0.4Λ, the Coupling Efficiency to this EDFA is shown by a dashed line and when the diameters of the air-holes in the last ring are increased to 0.8Λ, this is shown by a solid line. A log-scale is used for the coupling efficiency to show the lower value more clearly.

It can be observed that with the outer rings having larger air-holes, as the pitch length is reduced from 2.0 to 0.5 μm, the coupled power is seen to be stable over the range of lower values of pitch (for Λ = 0.7 – 1.0 μm) as shown by the solid line. In this case the value of the MFA of the PCF has an expanded, but also a stable value as shown earlier in Fig. 5, yielding a very stable power Coupling Efficiency with its maximum value of ~ 0.95 can be achieved at Λ = 0.85 μm.

However, the power coupling to an EDFA, for a PCF with all the air-holes identical (dashed line), not only shows a lower Coupling Efficiency but also shows a random variation in the coupling coefficient. This is due to the degeneration of the core mode with the cladding mode which is particularly frequent near cutoff. Previously it had been reported that a PCF near cutoff or when bent shows that the loss value is erratic due to mode degeneration [31,32] of the core mode with the surface modes in the extensive solid outer cladding. Similarly, it has been observed here that the presence of a larger air-hole reduces the silica area near the boundary and consequently reduces the possibility mode degeneration, resulting in a more stable in the coupling efficiency. Hence it is shown that by increasing the diameter of the last air-hole ring, the expanded modes are more isolated from the high index outer cladding region and mode degeneration is also avoided. Thus a stable coupling can be achieved over a range of the pitch lengths which is stable during the possible change of the pitch when the PCF is tapered. Such an approach would also be tolerant against misalignment, as the spot-size is expanded in this case.

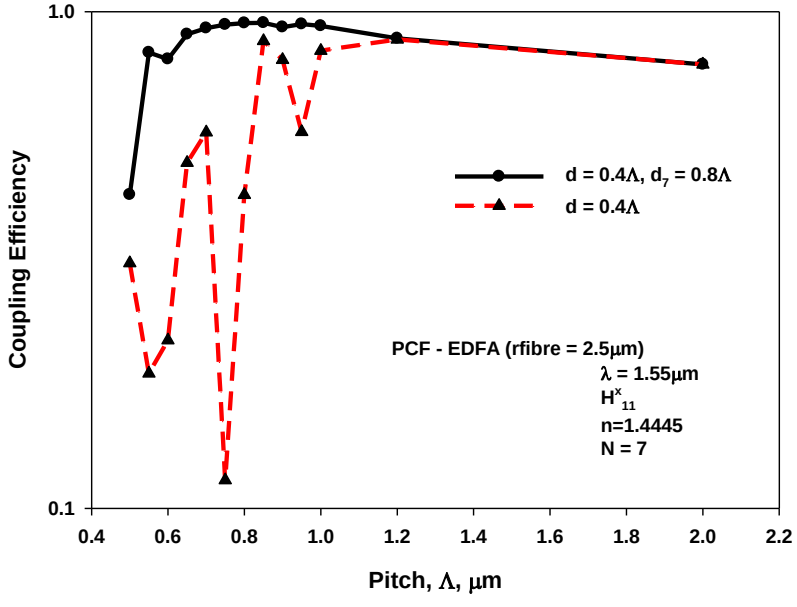

Fig. 6: Variations of the coupled power to a EDFA with the tapered pitch, Λ, of a PCF.

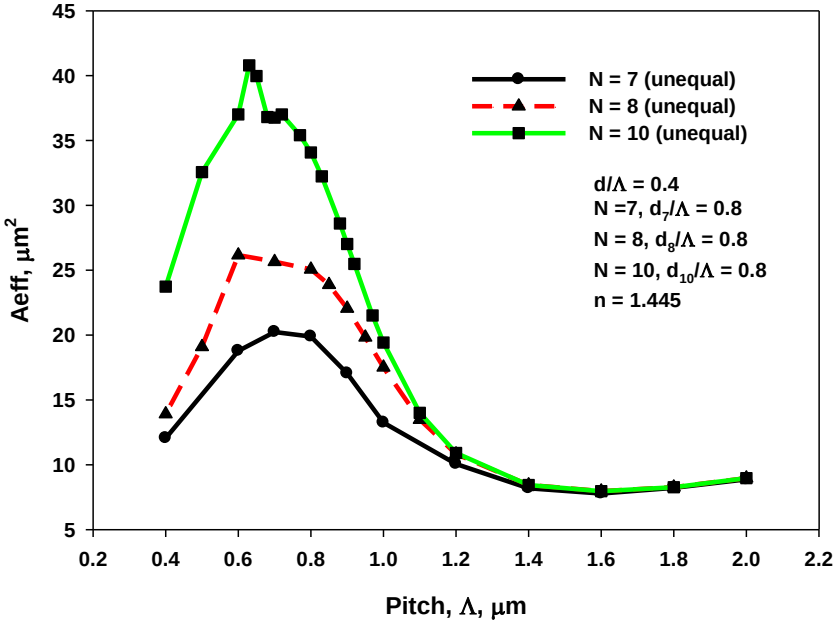

Fig. 7: Variations of the A_{eff} with the pitch length for PCFs having $d/\Lambda = 0.4$ and outermost $d/\Lambda = 0.8$ for N = 7, 8 and 10.

Next, the number of rings is increased to study the degree to which expansion of spot-size which can be achieved. The variation of the effective area, A_{eff} with the reduction of the pitch, Λ, is shown in Fig. 7 for N = 7, 8 and 10. In all the cases, the air-hole diameter of the last ring has been increased to 0.8Λ to stabilize the mode field area near their cutoff conditions.

In each case as the pitch is reduced, the MFA increases as the PCF designs approaches their cutoff, but due to the presence of larger air-holes in all the cases the MFA reaches a maximum value. However, it can be observed that for higher ring numbers, the maximum A_{eff} value was higher, which would allow efficient coupling to an optical fiber with a large MFA.

From the work done it is clear that different numbers of rings are best suited for coupling of a PCF to a SMF, EDFA or lensed fibre. Next, the mode shape area required from the different optical fibers, all of which guide a single moded waveguide, is studied by adjusting the radius and index contrast to maintain them identical. In this case, the cladding refractive index is taken as 1.445 and the core index is adjusted for each fiber diameter to have the same normalized dimension, V.

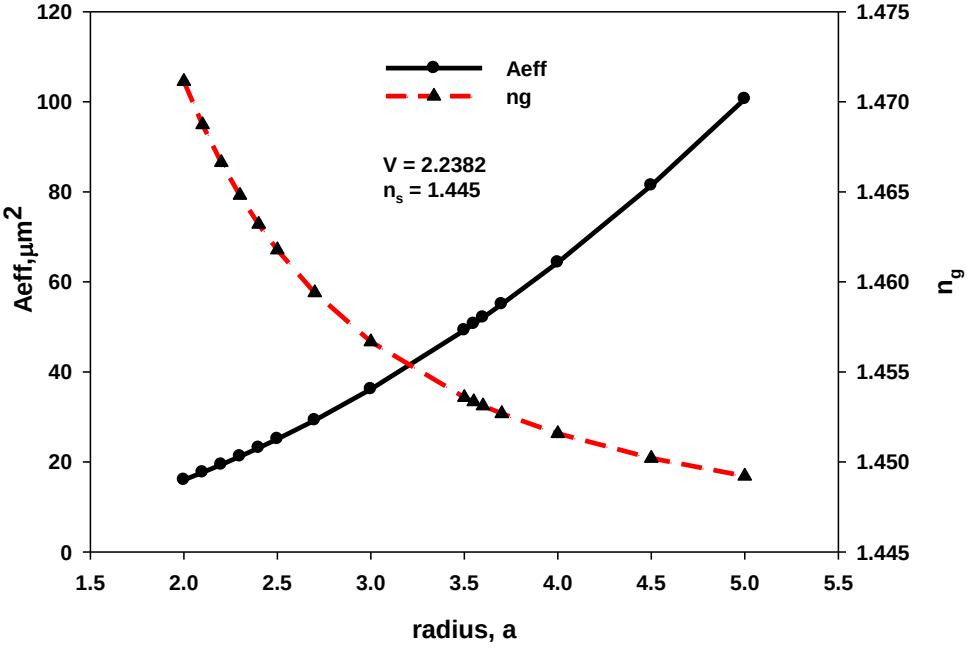

Fig. 8: Variation of A_{eff} and core refractive index difference, n_g of a SMF against fibre radius, a.

The variation of the required refractive index of the core with its radius, *a*, is shown in Fig. 8, designed to maintain the single modedness by keeping the V parameter fixed at V = 2.23821417, which is that of a typical SMF. The variation of the MFA, A_{eff} with the radius for this fiber with a constant value of V (where V= 2.23821417), is also shown here. It can be observed that as *a* is reduced, the value of A_{eff} also reduces.

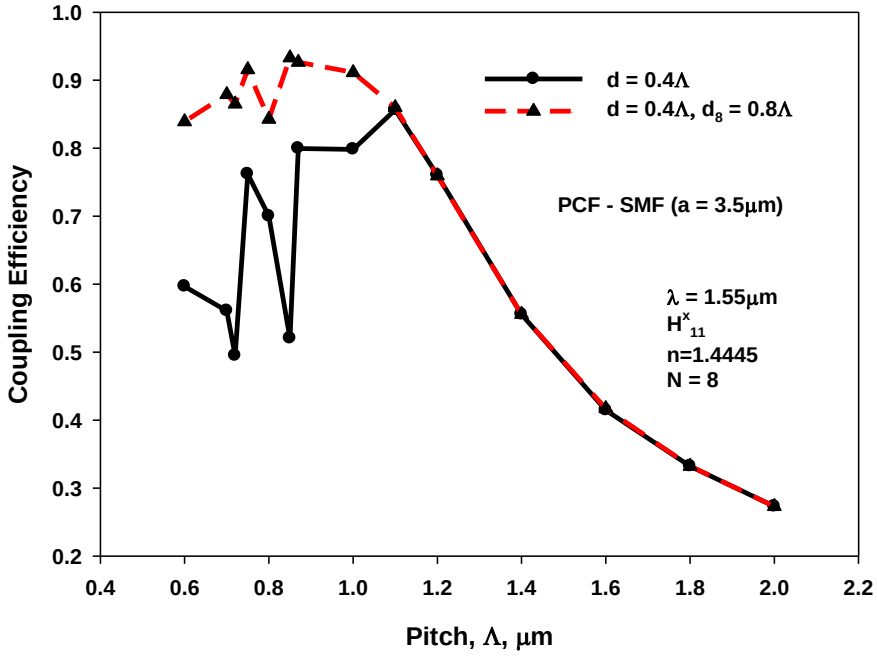

Fig. 9: Variation of Coupling Efficiency to PCF with tapered pitch, Λ and SMF, a = 3.5μm.

Next, the butt-coupling between a tapered PCF with N = 8 to an optical fiber with *a* = 3.5 μm (V = 2.23821417) is studied. The variation of the coupling efficiency of a PCF with N = 8 to an optical fiber with *a* = 3.5μm with the final pitch length, Λ, is shown in Fig. 9 for both equal air-holes and larger air-holes in the last ring (8^{th}) by a dashed and a solid line, respectively.

It is shown here that the maximum coupling efficiency (of 95%) can be achieved when the pitch length was 0.85 μm and butt-coupled to this fibre with *a* = 3.5μm. During the tapering process, if the pitch value change between 0.7 μm to 1.0 μm, the coupling efficiency will still be above 90%. This shows the design is very stable, with the possible adjustment of the terminating pitch length for a tapered PCF. However, using the design principle discussed, for coupling to a SMF, A_{eff} needs to be further increased to a value close to that of a SMF. As the number of rings is further increased, the expansion of the mode field profile closer to cutoff increases as well, hence, allowing for more effective coupling to a SMF.

Therefore, it can be seen that when a PCF is down-tapered for coupling, the variations in the dimensions of the pitch or the diameter of the air-holes that may arise as result of the fabrication or tapering process would not affect appreciably the power coupled between a PCF and an SMF or an EDFA.

3. CONCLUSION

A novel design approach for a PCF which could be considered as a candidate for efficient coupling to an optical fiber has been presented. Initially various MFA parameters and field profiles for a SMF and a PCF were studied. It has been shown here that a smaller air-hole diameter and a larger number of rings would allow the A_{eff} value to reach a higher value, which can be achieved by operating a PCF near cutoff. However, as its expansion near cutoff can be very rapid and unstable, by increasing the air-hole diameter in the last ring, this parameter can be stabilized with the variation of the fabrication tolerances. Using this approach presented above, it is possible to avoid uncertainty resulting from the variations in the dimensions of the pitch or the diameters of the air-holes in the PCF as a result of fabrication or tapering, thereby ensuring that the PCF can be successfully coupled to an optical fiber without any significant loss in coupled power. Additionally, it is also shown here that the largest air-holes in the last ring reduce the mode degeneration with the cladding modes. During the tapering process it has been assumed that the pitch, Λ, reduces gradually while keeping the d/Λ ratio constant. However, the air-holes can also collapse and the air-hole/pitch ratio can also change although this may give an additional flexibility but also an additional parameter to optimise the situation. Once the nature of the deviations are known *a priori* then a

rigorous numerical approach, such as that presented above, can be used to optimize the designs before their fabrication for experimental use. In this approach, as the PCF is operated near cutoff, it is normally expected that leakage loss and bending loss to be increased. However, in this approach since larger air-holes are used in the last ring, in fact, lower leakage and bending losses are expected. However, if required additional rings with larger air-holes can be included and the design can be optimized [34].

References

1. P. St.J. Russell, "Photonic-Crystal Fibers," J. Lightwave Technology, Vol. 24, No. 12, pp. 4729-4747, 2006.
2. P. Russell, "Photonic crystal fibers" Science, Vol. 299, No. 5605, pp. 358 -362, 2003.
3. N. A. Mortensen ,"Effective area of photonic crystal fibers," Optics Express, Vol. 10, No. 7, pp. 341-348, 2002.
4. B. T. Kuhlmey, R. C. McPhedran and C. M. de Sterke, "Modal cutoff in microstructured optical fibers," Optics Letters, Vol. 27, No. 19, pp. 1684-1686, 2002.
5. N. Kejalakshmy, B. M. A. Rahman, A. Agrawal, T. Wongcharoen and K. T. V. Grattan, "Characterisation of single-polarization single mode photonic crystal fiber using full-vectorial finite element method," Applied Physics B, Vol. 98, No. 1, pp. 223-230, 2008.
6. P. J. Bennett, T. M. Monro and D. J. Richardson, "Toward practical holey fiber technology: fabrication, splicing, modeling, and characterization," Optics Letters, Vol. 24, No. 17, pp. 1203-1205, 1999.
7. J. H. Chong and M. K. Rao, "Development of a system for laser splicing photonic crystal fiber," Optics Express, Vol. 11, No. 12, pp. 1365-1370, 2003.
8. Y. Wang, H. Bartelt, S. Brueckner, J. Kobelke, M. Rothhardt, K. Morl, W. Ecke, and R. Willsch, "Splicing Ge-doped photonic crystal fibers using commercial fusion splicer with default discharge parameters," Optics Express, Vol. 16, No. 10, pp. 7258-7263, 2008.
9. A.D. Yablon and R. T. Bise, "Low-loss high-strength microstructured fiber fusion splices using GRIN fiber lenses," IEEE Photonics Technology Letter, Vol. 17, No. 1, pp. 118-120, 2005.
10. J. Liu, T-H. Cheng, Y-K. Yeo, Y. Wang, L. Xue, Z. Xu, and D. Wang, "Light beam coupling between standard single mode fibers and highly nonlinear photonic crystal fibers based on the fused biconical tapering technique," Optics Express, Vol. 17, No. 5, pp. 3115-3123, 2009.
11. H. C. Nguyen, B. T. Kuhlmey, E. C. Magi, M. J. Steel, P. Domachuk, C. L. Smith and B. J. Eggleton, "Tapered photonic crystal fibres: properties, characterisation and applications", Applied Physics B, Vol. 81, No. 2 -3, pp. 377 – 387, 2005.
12. H. C. Nguyen, B. T. Kuhlmey, M. J. Steel, C. L. Smith, E. C. Magi, R. C. McPhedran and B. J. Eggleton, "Leakage of the fundamental mode in photonic crystal fiber tapers", Optics Letters, Vol. 30, No. 10, pp. 1123 – 1125, 2005.
13. J. K. Chandalia, B. J. Eggleton, R. S. Windeler, S. G. Kosinski, X. Liu, and C. Xu, "Adiabatic coupling in tapered air-silica microstructured optical fiber," IEEE Photonics Technology Letter, Vol. 13, No. 1, pp.52-54, 2001.
14. G. E. Town and J. T. Lizier, "Tapered holey fibers for spot-size and numerical-aperture conversion," Optics Letter, Vol. 26, No. 14, pp. 1042-1044, 2001.
15. S. G. Leon-Saval, T. A. Birks, W. J. Wadsworth, P. St. J. Russel, and M. W. Mason, "Supercontinuum generation in submicron fiber waveguides," Optics Express, Vol. 12, No. 13, pp. 2864-2869, 2004.
16. E. C. Magi, P. Steinvurzel, and B. J. Eggleton, "Tapered photonic crystal fibers," Optics Express, Vol. 12, No. 5, pp. 776-784, 2004.
17. B. M. A. Rahman, A. K. M. S. Kabir, M. Rajarajan, K. T. V. Grattan and V. Rakocevic, "Birefringence study of photonic crystal fibers by using the full-vectorial finite element method," Applied Physics B, Vol. 84, No. 1 -2, pp. 75 – 82, 2006.
18. T. Wongcharoen, B. M. A. Rahman, M. Rajarajan and K. T. V. Grattan, "Spot-size conversion using uniform waveguide sections for efficient laser-fiber coupling," Journal of Lightwave Technology, Vol. 19, No. 5, pp. 708–716, 2001.
19. M. Rajarajan, B. M. A. Rahman and K. T. V. Grattan, "Numerical study of spot-size expanders for an efficient OEIC to SMF coupling," IEEE Photonics Technology Letter, Vol. 10, No. 8, pp. 1082–1084, 1998.
20. P. E. Barclay, K. Srinivasan, M. Borselli and O. Painter, "Efficient input and output fiber coupling to a photonic crystal waveguide" Optics Letters, Vol. 29, No. 7, pp. 697 – 699, 2004.
21. H. Zhao, J. Zhang, G. Liu and Nelson Tansu, "Surface Plasmon dispersion engineering via double-metallic Au/Ag layers for III-nitride based light-emitting diodes", Applied Physics Letters, Vol. 98, No. 15, 151115, 2001.

22. C.H. Lu, C. C. Lan, Y. L. Li and C. P. Liu, "Enhancement of green emission from InGaN/GaN multiple quantum wells via coupling to surface plasmons in a two-dimensional silver array"' Advance Functional Materials, Vol. 21, No. 24, pp. 4719 – 4723, 2011.
23. J. J. Weirer, A. David and M. M. Megens, "III-nitride photonic-crystal light-emitting diodes with high extraction efficiency", Nature Photonics, Vol. 3, pp. 163 – 169, 2009.
24. X.H. Li, R. Song, Y. K. Ee, P. Kumnorkaew, J. F. Gilchrist and N. Tansu, "Light extraction efficiency of III-nitride light-emitting diodes with colloidal microlens array with various aspect ratios", Photonics Journal, Vol. 3, No. 3 pp. 489 – 499, 2011.
25. B. M. A. Rahman and J. B. Davies, "Finite-element solution of integrated optical waveguide," Journal of Lightwave Technology, Vol. 2, No. 5, pp. 682-688, 1984.
26. K. Saitoh and M. Koshiba, "Numerical Modelling of Photonic crystal fiber", Journal of Ligthwave Technology, Vol. 23, No. 11, pp. 3580 – 3590, 2005.
27. B. M. A. Rahman and J. B. Davies, "Analysis of optical waveguide discontinuities," Journal of Ligthwave Technology, Vol. 6, No. 1, pp. 52 – 57, 1988.
28. B. M. A. Rahman, E. O. Ladele, T. Wongcharoen and K. T. V. Grattan, "Spot-size converters for efficient laser-fiber coupling," Proc. SPIE vol. 4532, pp. 281 – 291, 2001.
29. M. Koshiba and K. Saitoh, "Structural dependence of effective area and mode field diameter for holey fibers", Optics Express, Vol. 11, No. 15, pp 1746 – 1756, 2003.
30. Encyclopaedia of Laser Physics and Technology, "Beam Radius"http://www.rp-photonics.com/beam_radius.html
31. B. M. A. Rahman, N. Kejalakshmy, M. Uthman, A. Agrawal, T. Wongcharoen and K. T. V. Grattan, "Mode degeneration in bent photonic crystal fibre study by using the finite element method," Applied Optics, Vol. 48, No. 31, G131-G138, 2009.
32. B. Bourliaguet, C. Pare, F. Emond, A. Croteau, A. Proulx, and R. Vallee, "Microstructured fiber splicing," Optics Express, Vol. 11, No. 25, pp. 3412-3417, 2003.
33. W. Jiang, L. Shen, D. Chen and H. Chi, "An extended FDTD method with inclusion of material dispersion for full-vectorial analysis of photonic crystal fibers", Journal of Lightwave Techonolgy, Vol. 24, No. 11, pp. 4417 – 4423, 2006.
34. B. M. A. Rahman, M. Uthman, N. Kejalakshmy, A. Agrawal, and K. T. V. Grattan, "Design of bent photonic crystal fiber supporting a single polarization", Applied Optics, Vol. 50 Issue 35, pp.6505-6511, 2011.